JOURNAL OF MATERIALS SCIENCE 31 (1996) 1027–1034

Effects of lithium addition and wheel velocity on the microstructure of aluminium–lithium alloy ribbons

M. HAJJAJI
Laboratoire de Chimie-Physique, Département de Chimie, Faculté des Sciences Sémlalia, B.P. S15, Marrakech, Maroc

L. CUTLER, G. L'ESPERANCE
(CM)², Ecole Polytechnique, Box 6079, Succ. A, Montréal, Canada H3C 3A7

The effects of Li addition and wheel velocity on the microstructure of as-cast Al–Li ribbons were studied by optical metallography, scanning and transmission electron microscopy and by X-ray diffraction. Li addition has a marked effect on the ribbon solidification mechanism. Ribbons spun at 12.5 m s^{-1} and which contained up to 1.79 wt% Li experienced a cooling rate of about 10^4 K s^{-1} and solidified under the melt jet with a growth rate greater than 0.3 m s^{-1}. However, when Li content exceeded about 3 wt%, the ribbons were undercooled (cooling rate $\approx 10^6$ K s^{-1}) and formed far from the melt puddle effect. Under these conditions, unusual secondary featureless zones occurred through the ribbon thickness and the detected phases corresponded to those expected to be formed under equilibrium conditions. Nevertheless, δ' (Al_3Li) phase did not occur in ribbons containing up to 1.79 wt% Li or in the featureless zones of the most Li-rich ribbons (Li > about 3 wt%). Changing of the wheel velocity from 12.5 to 22.2 or 35.7 m s^{-1} did not affect the ribbon formation mechanism, but it favoured the δ' precipitation and decreased slightly the grain size.

1. Introduction

Lithium addition to aluminium based alloys reduces their density and increases their elastic modulus. These lighter alloys have high technological potential in the aircraft frames industry. However, processing problems lead to alloys having low ductility and fracture resistance when conventional techniques are used. In order to improve their mechanical properties several studies have been performed on Al–Li specimens prepared from ingots or pieces of consolidated rapidly solidified powder [1–6]. Nevertheless, few investigations have been performed on the microstructure of as-cast Al–Li alloys produced by rapid solidification using atomization or melt spinning techniques [7, 8].

The aim of this work is to study the effects of Li addition and wheel velocity on the microstructure of as-cast Al–Li ribbons produced by the free-jet melt spinning (FJMS) technique. This study may help to optimize the as-solidified structure and allow one to follow the microstructure evolution in the consolidated materials. Moreover, it is an attempt to understand the formation process of ribbons produced by chilled block melt spinning.

2. Experimental procedures

Ribbons of binary aluminium–lithium alloys, containing up to 10 wt% Li (approximately 30 at%), were prepared from pure metals (Al 99.999%; Li 99.9%) by the free-jet melt spinning technique [9]. The total charge used in each run was around 3 g. The casting wheel temperature T_S and the melt superheat ΔT were kept constant (T_S = 298 K; ΔT = 71 K) and the tangential wheel velocities 12.5, 22.2 and 35.7 m s^{-1} were used. The average ribbon thickness ($\bar{t}$ in μm) may be estimated from the empirical relationship [9]:

$$\bar{t} = 575 \times V_S^{-0.9}$$

where V_S is the wheel speed (in m s^{-1}). Further details on the processing conditions are reported elsewhere [10].

Since a part of the study focused on the effects of Li addition, the actual Li composition in the ribbons, which is also the nominal one, was determined by atomic absorption spectroscopy.

Etched longitudinal sections of as-cast ribbons were examined by optical metallography and their chilled and free surfaces were monitored using a Jeol 820 scanning electron microscope (SEM).

In order to investigate the microstructure in the cross-section of as-cast ribbons, thin foils from the chilled and free surfaces and also from the mid-thickness regions were prepared by twin jet electropolishing. The undesired ribbon side was coated with a lacquer and the perforation position was scrupulously controlled by optical microscopy. The thin foils were examined by a Jeol 2000FX transmission electron microscope (TEM) operating at 200 kV.

0022–2461

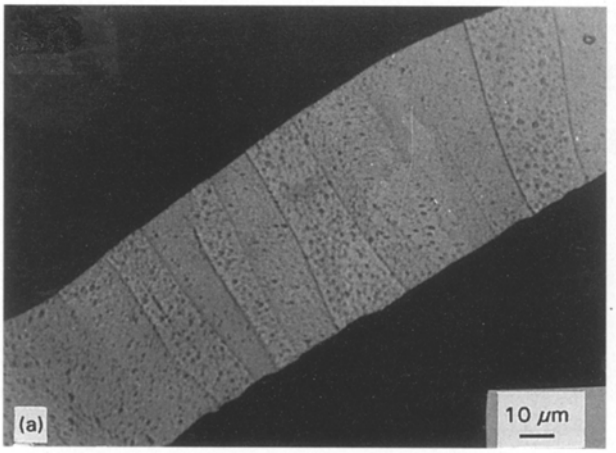

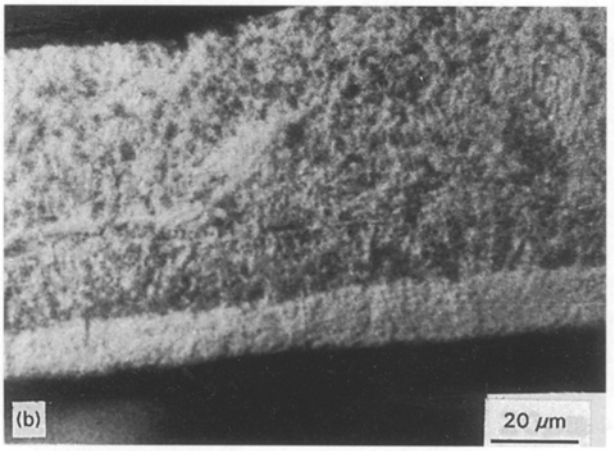

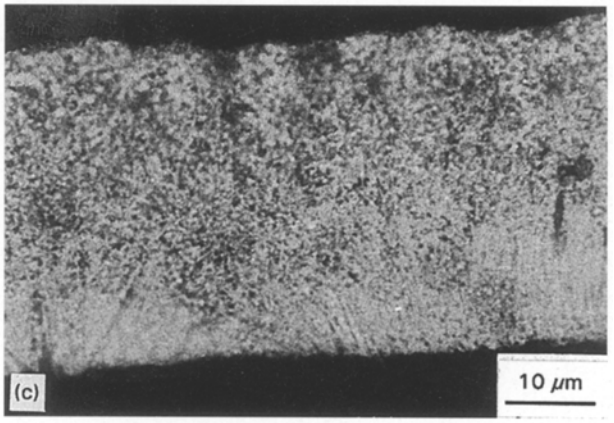

Figure 1 Longitudinal sections of as-cast ribbons: (a) 1.2 wt % Li; (b) 4.6 wt % Li; and (c) 9.91 wt % Li (chilled side at bottom).

Texture characterization and phase identification were performed by X-ray diffraction using a Phillips diffractometer with CuK_α radiation.

3. Results

3.1. Effects of Li addition on the microstructure of ribbons spun at 12.5 m s^{-1}

3.1.1. Optical metallography

The microstructure seen across the ribbon thickness changes strongly above a certain amount of added Li. Up to 1.79 wt % Li, ribbons were mainly constituted of large columnar grains. A typical micrograph is shown in Fig. 1a. However, when the Li content

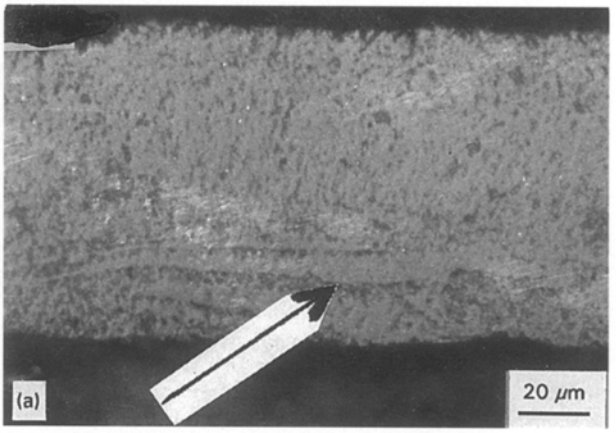

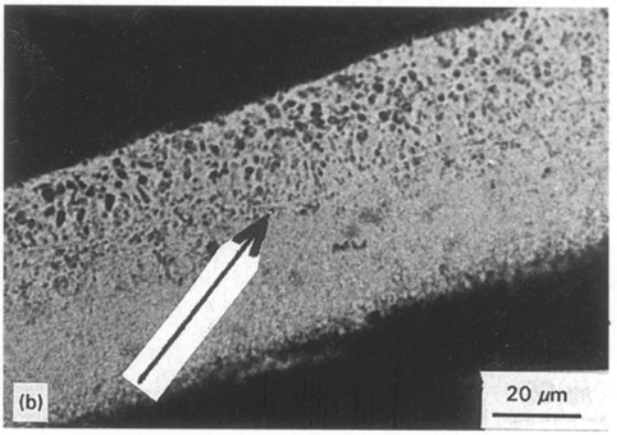

Figure 2 Secondary featureless zones (non-etched bands) in longitudinal sections of ribbons: (a) 4.6 wt % Li; and (b) 9.91 wt % Li (wheel side at bottom).

exceeds about 3 wt %, two distinct zones were formed (Fig. 1b): a well-defined featureless band near the wheel side is adjacent to a cellular/dendritic structure. At times, radial columns, as shown in Fig. 1c, occurred near the chilled surfaces of 4.6 and 9.91 wt % Li ribbons.

It is worth mentioning that, in addition to the occurrence of the principal featureless zone, non-etched fine bands, as indicated by arrows in Fig. 2, were particularly developed in 4.6 and 9.91 wt % Li ribbons. As can be seen in Fig. 2a, the manifestation of these secondary featureless zones seems to be dependent upon the nature of the contact between the ribbon and wheel surfaces.

3.1.2. TEM examinations

TEM investigations performed on thin foils prepared from the chilled side and the mid thickness region of ribbons containing up to 1.79 wt % showed that the size and morphology of the grains was less affected by Li addition. Moreover, they exhibited large hexagonal section grains of around 10 μm in size (Fig. 3a) which were exempt from precipitation. However, a substructure (Fig. 3b), as well as scarce and very fine precipitates which were identified as δ (AlLi) phase, was formed only near the unchilled side of 1.79 wt % Li ribbon. On the other hand, grains in ribbons with Li

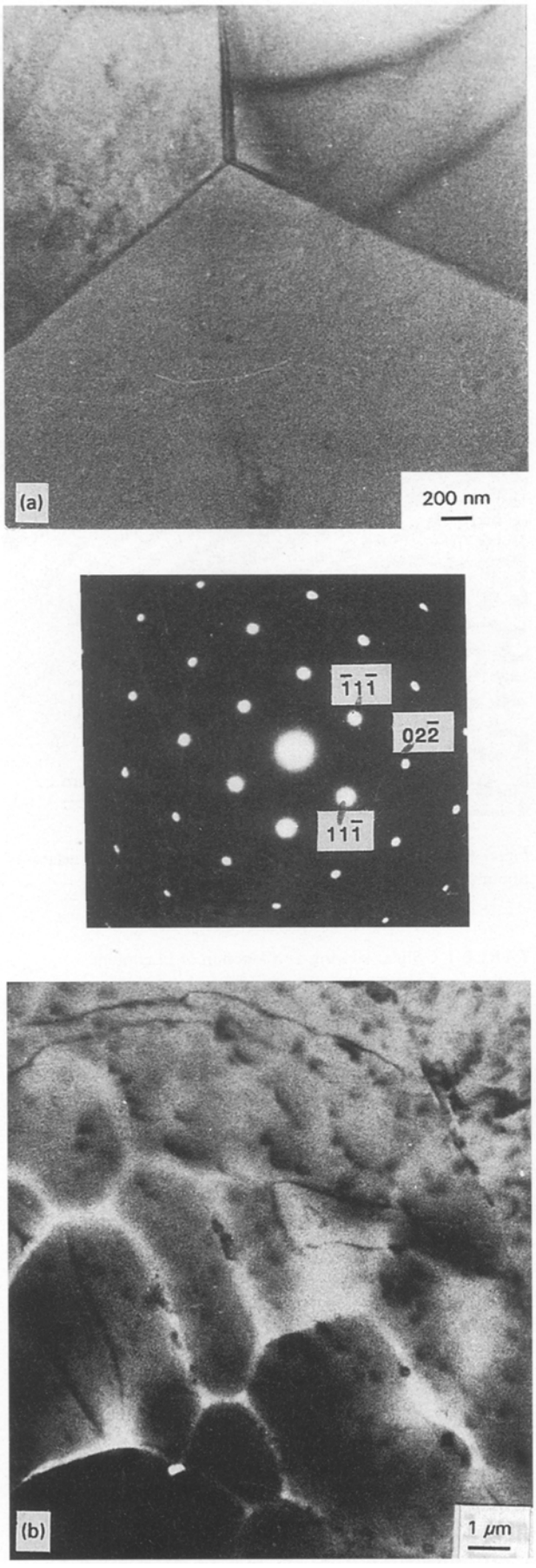

Figure 3 Microstructure of 1.79 wt % Li ribbon: (a) mid thickness region and associated diffraction pattern (zone axis: $[0\,1\,1]_\alpha$); and (b) free side.

content ≥ 3 wt % had different sizes and morphologies as compared to those seen previously. Small precipitation-free grains (around 0.2 μm in size) appeared near the wheel side surfaces of 3.14 and 4.6 wt % Li ribbons. A typical microstructure and its associated SAD pattern are shown in Fig. 4a (the intragranular contrast seen in this micrograph is due to dislocation loops). Cellular substructure similar to that in Fig. 3b as well as abundant precipitates of δ′ (Al_3Li) phase (Fig. 4b) were, however, formed in the close atmosphere side region.

3.1.3. SEM investigations

SEM examinations conducted on those chilled surface areas which displayed a perfect contact with the wheel surface showed the existence of oriented bands formed by juxtaposed elongated grains (Fig. 5). However, in the depressed regions (gas pockets) of the chilled surface, a cellular/dendritic structure occurred (Fig. 6). The cell/dendrite tips grew preferentially towards the depth of the gas pockets (i.e. towards the unchilled

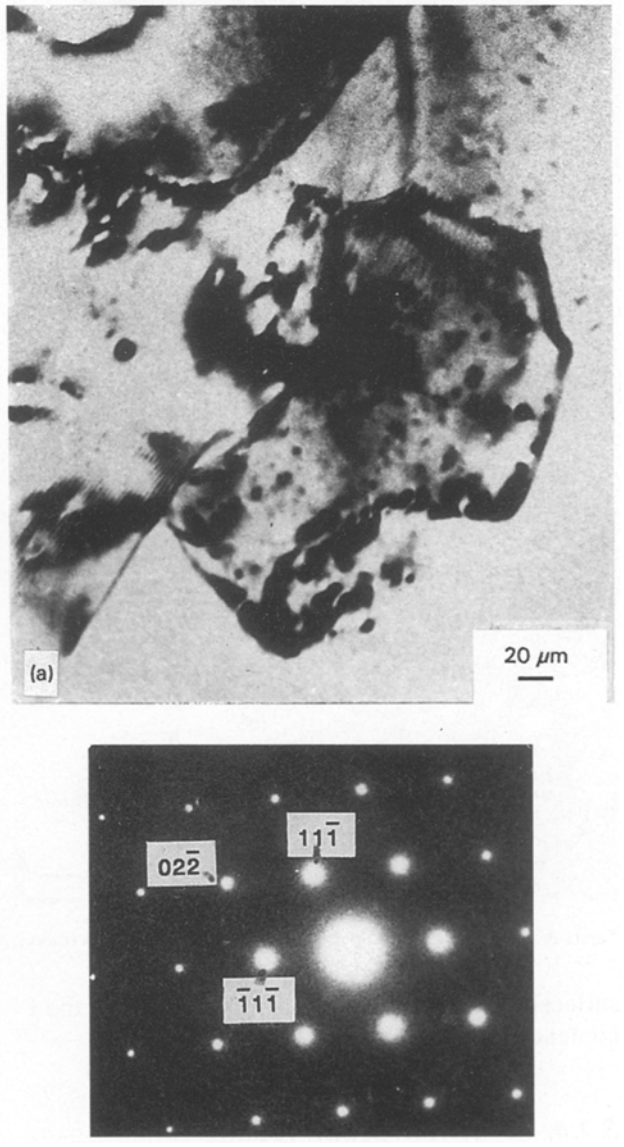

Figure 4 TEM micrographs of 3.14 wt % Li ribbon: (a) wheel side and associated diffraction pattern (zone axis: $[0\,1\,1]_\alpha$); and (b) unchilled side and associated diffraction pattern ($[0\,1\,1]_\alpha // [0\,1\,1]_\delta$).

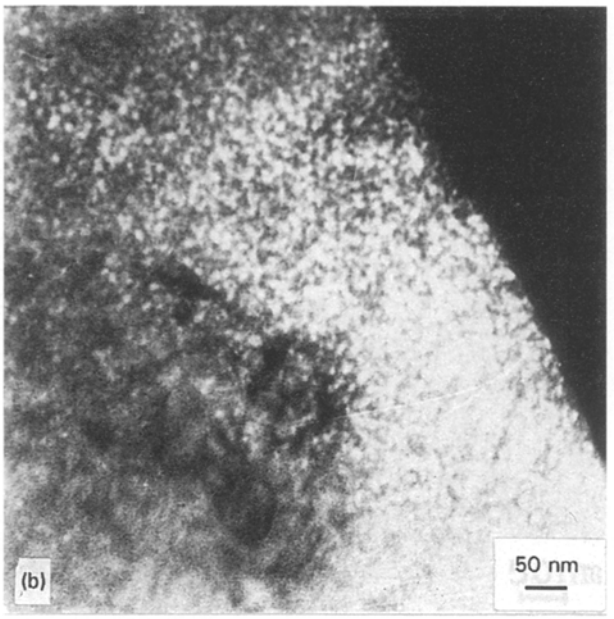

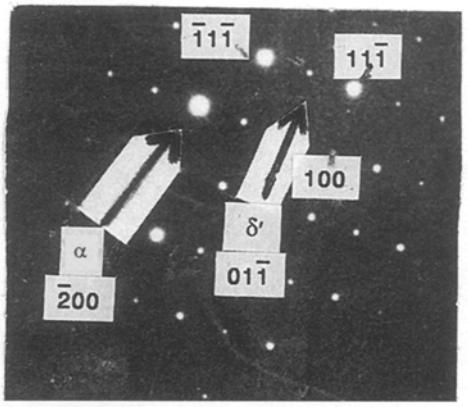

Figure 4 (continued).

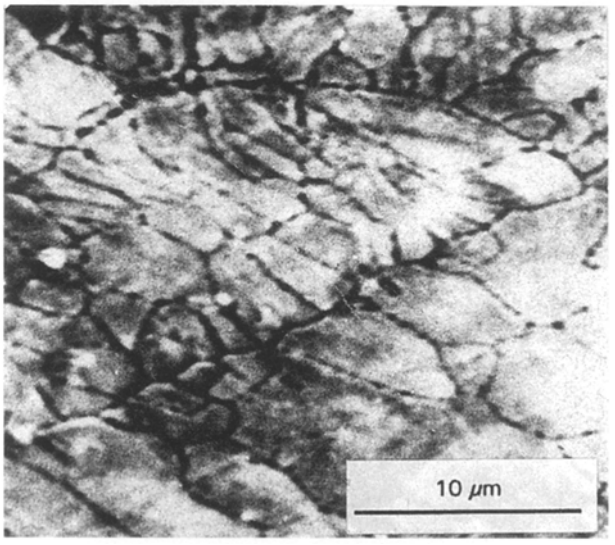

Figure 5 Elongated grains in the chilled surface of 4.6 wt % Li ribbon.

surface). The average cell spacing decreases as the Li content increases (Table I).

3.1.4. X-ray diffraction results

The free and chilled surfaces of each as-spun ribbon were examined by X-ray diffraction. The identified phases are reported in Table II.

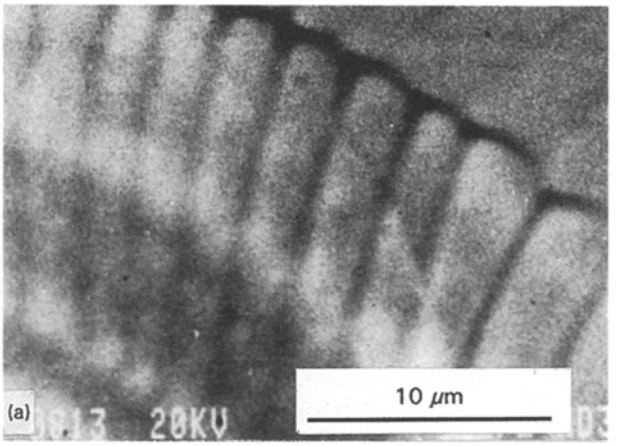

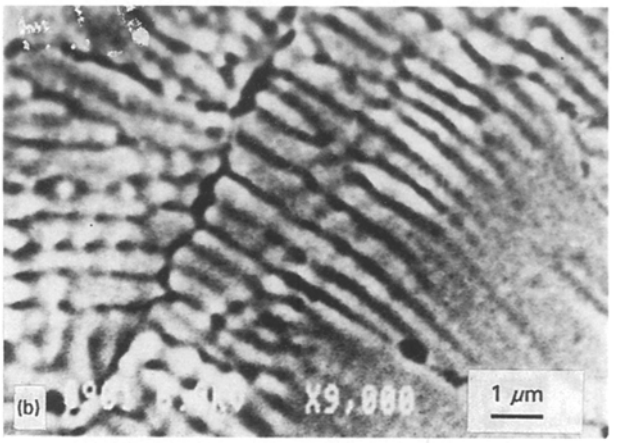

Figure 6 Microstructure of depressed areas in the chilled surfaces of ribbons; (a) 1.2 wt % Li; (b) 4.6 wt % Li.

TABLE I Cellular spacing as a function of Li content

Li content (wt %)	1.2	1.79	3.14	4.6
Cell spacing (μm)	2.7	2.2	0.7	0.5
Standard deviation: σ (μm)	0.2	0.3	0.1	0.2

TABLE II Phases in as-cast Al–Li ribbons

Li content (wt % Li)	Wheel side	Free side
1.2	α	α
1.79	α	α, δ
3.14	α, δ, δ′	α, δ, δ′
4.60	α, δ	α, δ
9.91	α, δ	α, δ

These results show that each ribbon contains the same phases in both surfaces except for 1.79 wt % Li ribbon. Further, δ′ phase which was observed by TEM in 4.6 and 9.9 wt % Li ribbons was not detected by X-ray diffraction because the amount present was probably below the detection threshold.

To follow the effects of Li addition on the evolution of ribbon texture, the X-ray intensities I_{001} and I_{002} diffracted by (0 0 1) and (0 0 2) planes of α phase were measured and the ratio I_{002}/I_{001} was determined. As seen in Fig. 7 the ribbon texture decreases

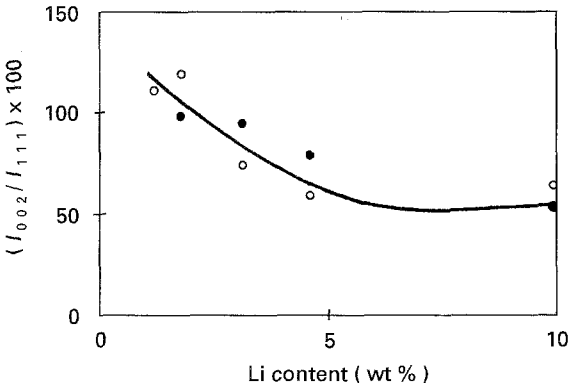

Figure 7 Effect of Li addition on texture.

with Li content and tends finally to be the same as that of a powdery specimen of pure aluminium.

3.2. Effects of wheel velocity on Al–Li ribbons microstructure

Noting that the microstructure changed when the Li content exceeded 1.79 wt %, the effects of wheel velocity on ribbon microstructures were tested using two compositions: 1.6 and 3.3 wt % Li.

3.2.1. Ribbons with less than 1.79 wt % Li (1.6 wt %)

Increases in wheel velocity did not have a substantial effect on grain morphology but it reduced the ribbon thickness and affected the grain size (Fig. 8). Further, the mean cell spacing at 35.7 m s^{-1} ($\lambda = 0.8$ μm; $\sigma = 0.2$ μm) is around a third of that determined at 12.5 m s^{-1} ($\lambda = 2.2$ μm; $\sigma = 0.1$ μm).

TEM investigations conducted on thin foils prepared from different layers through the ribbon thickness showed that δ′ precipitates spread through the thickness as the wheel speed increased from 22.2 to 35.7 m s^{-1}.

3.2.2. Ribbons with more than 1.79 wt % Li (3.3 wt %)

The occurrence of the segregated and featureless zones was not affected by the changes in wheel velocity. However, as seen in Fig. 9, the width (W) of the featureless zone increases with the wheel speed (V_S). These variations may be expressed by the empirical equation:

$$\frac{W}{t} = (0.4\ V_S + 33)10^{-2}$$

where t is the ribbon thickness (V_S is in m s^{-1}).

Fine precipitates of δ′, as shown in Fig. 10a, were detected through the thickness of ribbons prepared at 22.2 and 35.7 m s^{-1} and also in the segregated part of the ribbon spun at 12.5 m s^{-1}. In addition, coarse precipitates of δ phase (Fig. 10b) were developed in all the segregated regions of these ribbons.

As a consequence of the increases in wheel velocity, the secondary featureless zones are formed even near the unchilled ribbon surface (Fig. 11).

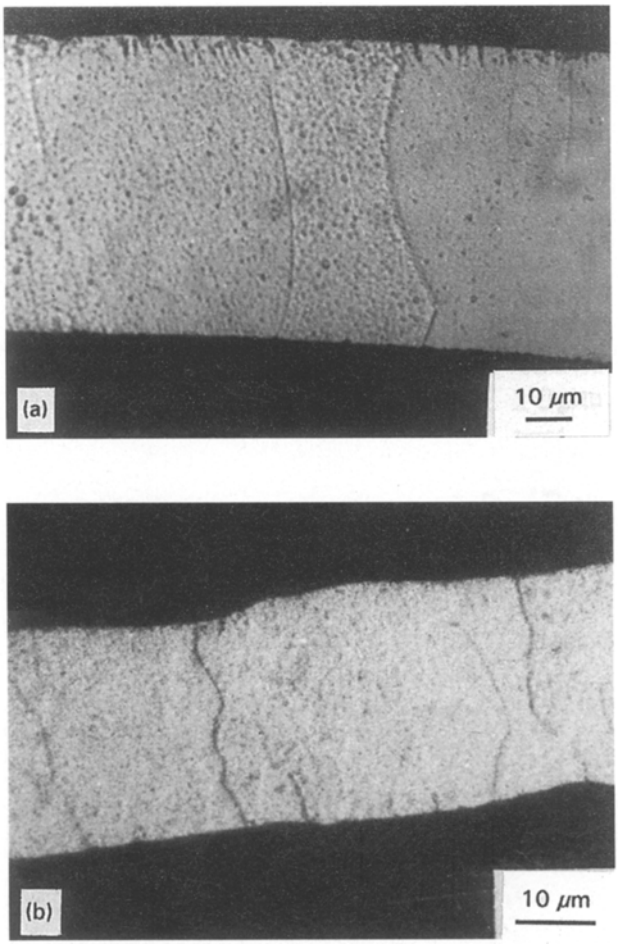

Figure 8 Longitudinal sections of 1.6 wt % Li ribbons spun at (a) 12.5 m s^{-1} and (b) 35.7 m s^{-1} (wheel side at bottom).

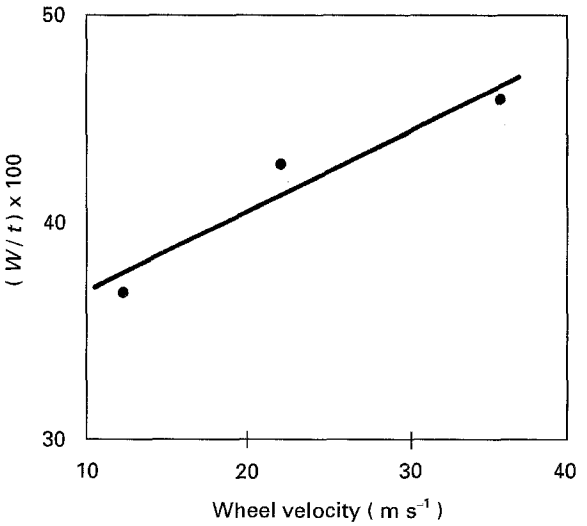

Figure 9 Effect of wheel velocity on featureless zone width.

4. Discussion

4.1. Solidification mechanism of ribbons spun at 12.5 m s^{-1}

Except for the occurrence of the unusual secondary featureless zones in samples containing more than 3 wt % Li, the microstructure which was formed through the cross-sections of these ribbons is similar to that which occurred in as-spun ribbons produced by the melt spinning technique [11].

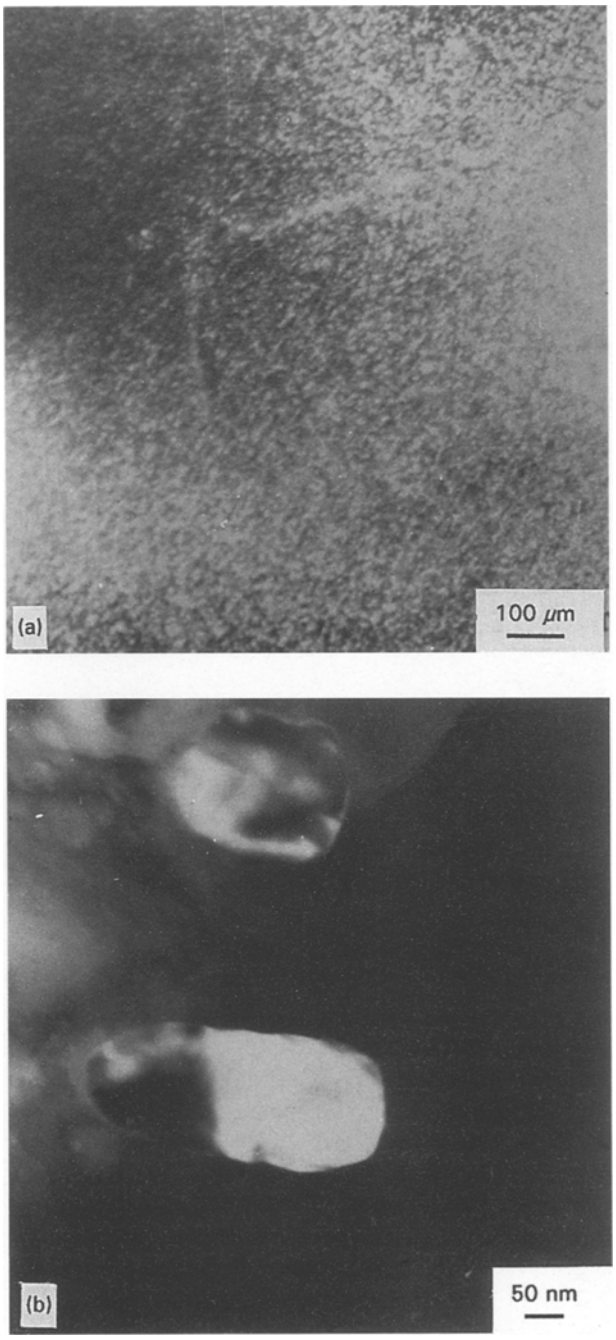

Figure 10 Dark field images of the unchilled side of 3.3 wt % Li ribbon (wheel speed: 35.7 m s^{-1}): (a) δ′ phase (1 0 0 reflection, zone axis: [0 0 1]); and (b)δ phase (1 1 $\bar{1}$) reflection, zone axis; [0 1 1]).

4.1.1. Ribbons with Li content ≤ 1.79 wt %

Since columnar grains can grow into a flowing melt (such as the melt puddle) [12] and since ribbons containing less than 1.79 wt % Li are constituted of columnar grains, and fairly uniform from one side to the other (Fig. 1a), these ribbons seem to have solidified under the melt puddle. Under such conditions, nuclei developed on the chilled substrate surface and grew as columnar grains because of the high rate of heat extraction and the high positive thermal gradient experienced by the melt puddle. However, grain growth is mainly controlled by the rate of heat extraction via the ribbon/substrate interface.

4.1.1.1. Estimation of the mean cooling rate. The mean cooling rate ($\dot{T}$) is estimated from the empirical relation

$$\lambda = A\dot{T}^{-n}$$

which is widely applied for binary Al–X alloys [13–15]. λ is the measured cell spacing reported in Table I. $A \approx 50\ \mu m\ (K\ s^{-1})^{1/3}$ and $n \approx 1/3$. The estimated $\dot{T}$ for ribbons containing up to 1.79 wt % Li does not exceed $2 \times 10^4\ K\ s^{-1}$.

4.1.1.2. Determination of the growth rate. Assuming that prior undercooling of the melt is negligible, the average growth rate (R) may be calculated from the expression:

$$R = \dot{T}(\Delta T/h_P)^{-1}$$

where h_P is the melt puddle height ($h_P \approx 2$ mm). The calculated R for ribbon areas which exhibited a poor contact with the chilled surface (gas pocket areas) is about 0.3 m s^{-1}. Its value for perfect contact regions is obviously much greater.

When ribbons solidified under the melt jet, the released heat was extracted through the solid/wheel surface interface. Assuming that the thermal gradient in the formed solid is negligible and the cooling process is Newtonian, the growth rate also can be estimated from the relation:

$$R = \frac{h(T_L - T_S)}{\rho L + \rho C_P(T_L - T_M)}$$

with h: interfacial heat transfer coefficient; $h = 10^5$–$10^6\ W\ m^{-2}\ K^{-1}$ [16]. T_L: liquid temperature; T_S: substrate temperature; T_M: melting temperature; C_P: specific heat of the melt, $C_P = 1.091 \times 10^3\ J\ kg^{-1}\ K^{-1}$ [17]; L; latent heat, $L = 3.95 \times 10^5\ J\ kg^{-1}$ [17]; ρ: alloy density. For good contact areas the heat transfer coefficient is about $10^6\ W\ m^{-2}\ K^{-1}$ [16, 18] and the calculated maximum growth rate is around 0.5 m s^{-1}. As compared to the previous results, this solidification rate is realistic. However, because of the gas pockets, the heat transfer must be reduced ($h < 10^6\ W\ m^{-2}\ K^{-1}$). In this latter case, assuming that $h = 2 \times 10^5$ to $5 \times 10^5\ W\ m^{-2}\ K^{-1}$, the calculated growth rate is comparable with that previously established.

Texture examination showed that the elongated grains seen across the thickness of the ribbons containing up to 1.79 wt % Li grow preferentially in ⟨1 0 0⟩ directions. This preferred growth direction which corresponds to the heat transfer direction is often encountered in conventionally cast F C C or C C metals [19].

The phase detection difference observed for the two sides of 1.79 wt % Li ribbon (Table II) is due to X-ray penetration. For example, when the X-ray angle of detection is 20° and the fraction of the total diffracted intensity which is contributed by a ribbon layer is 95%, the depth of X-ray penetration is 48 μm. This value is small compared to the average ribbon thickness which is about 60 μm. δ and α phases occurred simultaneously near the unchilled side of 1.79 wt % Li ribbon when the enriched solute layer in front of the

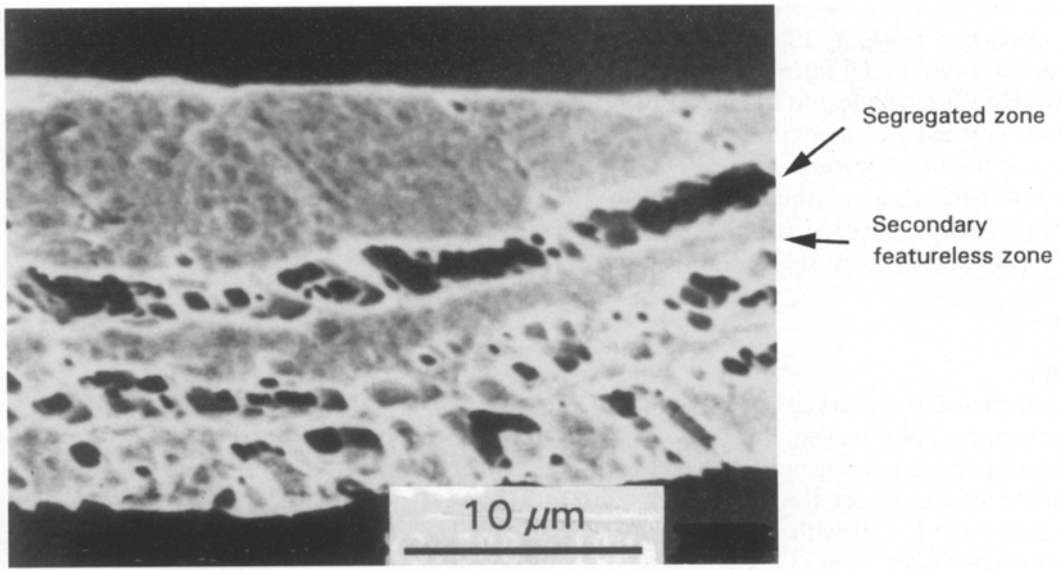

Figure 11 Secondary featureless zones in 3.3 wt % Li ribbon spun at 22.2 m s^{-1} (wheel side at top).

liquid/solid interface is solidified, once the effects of recalescence phenomenon and melt superheat as well as the distance from the heat sink block become relatively important.

4.1.2. Ribbons with Li content >3 wt %

The cross-section of ribbons containing more than 3 wt % Li exhibited featureless and segregated zones. Because the featureless zones are a melt undercooling manifestation [20] and since the melt cannot be supercooled under the liquid jet [21], these ribbons probably supercooled and solidified away from the melt puddle effect. This phenomenon is attributed to the solute addition which can depress the nucleation temperature as it does the liquidus temperature [22, 23]. Indeed, the calculated cooling rate for these ribbons is about 100 times that determined for ribbons containing up to 1.79 wt % Li. Thermodynamically, the partitionless solidification (as in the featureless band) in Al–Li alloys containing up to 20 wt % Li required an undercooling >30 K. Such values can be attained by the melt spinning technique [18, 20].

The existence of numerous dispersed catalytic sites (imperfections, oxides, etc) on the wheel surface allowed heterogeneous nucleation in the 9.9 wt % Li quenched melt and therefore radiating grains occurred at different places in the chilled side. The same radiating growth was observed in solidified undercooled melt droplets [24].

The occurrence of secondary featureless zones is also an indication of the melt supercooling. Presumably, their alternate formation across the ribbon thickness may result from the growth velocity changes during solidification of the undercooled melt.

SEM examinations performed on ribbon surfaces showed perforations with Li content >about 3 wt %. These may be taken as another sign of the melt supercooling. The trapped gas, rotating with the wheel surface, is subject to high temperature and pressure. Therefore, it can escape more easily through the thin undercooled melt layer which is extracted from the bottom of the melt puddle leading to perforations. However, it seems unlikely that this process would happen under the melt jet.

TABLE III Effect of the wheel speed on ribbon cooling rate

V (m s^{-1})	12.5	22.2	35.7
λ (μm)	2.2	1.6	0.8
σ (μm)	0.2	0.2	0.1
$\dot{T}$ (K s^{-1})	1.2×10^4	3×10^4	2.4×10^5

The texture reduction due to the Li addition (Fig. 7) is related to the increasing width of the featureless zone which is described as a randomness region [25]. Moreover, the texture may be decreased when grains are developed in the quenched melt, near the unchilled side.

4.2. Effects of the wheel velocity

Given the similarity between the microstructure of 1.6 wt % Li ribbons spun at 12.5, 22.2 and 35.7 m s^{-1} and according to the results previously reported, these ribbons are solidified under the melt puddle regardless of the wheel velocity. However, a change in wheel velocity affects the cooling rate (Table III) and also the grain size.

The gas layer rotating with the substrate is reduced when the wheel velocity increases and therefore the heat transfer coefficient and the cooling rate increase.

Referring to the miscibility gap ($\alpha + \delta'$) of Al–Li phase diagram [26] and since δ' appeared in 1.6 wt % Li ribbons spun at 22.2 and 35.7 m s^{-1}, the final temperature reached by these ribbons was probably less than 455 K. Indeed, the higher the substrate speed, the smaller the contact time between the solidified ribbon and the wheel surface. Therefore, at high wheel speeds the temperature of the ejected ribbon was still high and the cooling process continued slowly in the ribbon recuperation chamber.

The wheel speed did not affect the formation of the featureless and segregated zones in 3.3 wt % Li ribbons and consequently the ribbon formation process seems unchanged. However, the featureless width increases with the wheel speed because of the increase in the heat transfer coefficient magnitude. Morevoer, δ' formation in the featureless zones of ribbons prepared at 22.2 and 35.7 $m\,s^{-1}$ may have occurred by precipitation from the supersaturated α-Al solid solution.

5. Conclusions

Changes in Li content have a marked effect on the solidification mechanism. For a tangential velocity of 12.5 $m\,s^{-1}$ and for ribbons containing up to 1.79 wt % Li, the solidification occurs under the melt puddle (cooling rate is about $10^4\,K\,s^{-1}$) with an estimated solidification rate greater than 0.3 $m\,s^{-1}$. The microstructure of these ribbons consisted of mainly columnar grains without δ' precipitation. On the other hand, when Li concentrations exceed 3 wt %, the ribbons exhibit a microstructure characteristic of ribbons that rapidly solidify away from the effects of the puddle (the estimated cooling rate is $10^6\,K\,s^{-1}$). For these ribbons, Li additions favour the undercooling of the liquid and decrease the solid nucleation temperature. This results in a microstructure which consists of a featureless zone near the chill block followed by a segregated zone near the free ribbon surface. At times, these zones alternated forming secondary featureless zones. No precipitate was detected in the featureless zone but δ' and δ were developed in the segregated region.

Changing the tangential wheel speed from 12.5 to 22.2 or 35.7 $m\,s^{-1}$ did not affect the ribbon formation mechanism. However, it modified the process of precipitation.

References

1. T. H. SANDERS Jr, and E. A. STARKE, Jr (Eds), "Aluminium–Lithium I" (TMS-AIME, Warrendale, PA, 1981).
2. *Idem*, "Aluminium–Lithium II" (TMS-AIME, Warrendale, PA, 1984).
3. C. BAKER, P. J. GREGSON, S. J. HARRIS and C. J. PEEL (Eds), "Aluminium–Lithium III" (Institute of Metals, London, 1986).
4. G. CHAMPIER, B. DUBOST, D. MIANNY and L. SALETAY (Eds), Proceedings of the 4th International Al–Li Conference, France, 1987 (Les Editions de Physqiue, Paris, 1987).
5. T. H. SANDERS, Jr and E. A. STARKE, Jr (Eds), "Aluminium–Lithium V" (Materials and Component Engineering Publications Ltd, Birmingham, UK, 1989).
6. M. PETERS and P. J. WINKLER (Eds), "Aluminium–Lithium VI" (FRG, 1991).
7. F. H. SAMUEL and G. CHAMPIER, *Z. Metallkd.* **78** (1987) 670.
8. D. H. KIM, B. CANTOR and H. I. LEE, *J. Mater. Sci.* **23** (1988) 1695.
9. M. HAJJAJI, L. CUTLER and G. L'ESPÉRANCE, *J. Alloys Compounds* **188** (1992) 194.
10. L. R. CUTLER, M. HAJJAJI and G. L'ESPÉRANCE, in "Aluminium–Lithium V" edited by T. H. Sanders, Jr and E. A. Starke, Jr (Materials and Component Engineering Publications Ltd, Birmingham, UK, 1989) p 113.
11. H. JONES, *Mater. Sci. Eng.* **65** (1984) 145.
12. R. ICHIKAWA, H. TANIGUCHI and O. ASAI, *Z. Metallkd* **71** (1980) 260.
13. H. JONES, "Rapid Solidification of Metals and Alloys" Monograph 8 (Institution of Metallurgists, London 1982).
14. H. MATYJA, B. C. GIESSEN and N. J. GRANT, *J. Inst. Metals* **96** (1968) 30.
15. S. J. SAVAGE, D. ELIEZER and F. H. FROES, *Metall. Trans. A* **18A** (1987) 1533.
16. R. MEHRABIAN, *Int. Metals Rev.* **27** (1982) 185.
17. H. F. SAMUEL, *Metall. Trans. A* **17A** (1986) 73.
18. T. W. CLYNE, *Metall. Trans. B.* **15B** (1984) 369.
19. M. MATSUURA, in "Rapidly Quenched Metals V", edited by S. Steeb and H. Warlimont (North-Holland, Amsterdam, 1985) p. 261.
20. C. HAYZELDEN, J. J. RAYMENT and B. CANTOR, *Acta Metall.* **31** (1983) 379.
21. H. H. LIEBERMANN and R. J. BYE, Jr, in "Rapidly Solidified Crystalline Alloys" edited by S. K. Das, B. H. Kear and C. M. Adam (Metallurgical Society/AIME, Warrendale, PA, 1985) p. 61.
22. J. H. PEREPEZKO, *Mater. Sci. Eng.* **65** (1984) 125.
23. M. C. FLEMINGS and Y. SHIOHARA, *ibid.* **65** (1984) 157.
24. C. CESAR, W. KOSTER, R. WILLNECKER and D. M. HERLACH, *ibid.* **98** (1988) 339.
25. S. N. TEWARI, *Metall. Trans. A* **19A** (1988) 1711.
26. D. R. LIU and D. B. WILLIAMS, *Scripta Metall.* **22** (1988) 1361.

Received 22 July 1994
and accepted 17 July 1995